Electronic Supplementary Information

DC bias characteristic enhancement of the powder core by using densified submicron sized FeNi particles through spray pyrolysis

Eka Lutfi Septiani [a,b], Jun Kikkawa [a], Kiet Le Anh Cao [a], Tomoyuki Hirano [a], Nobuhiro Okuda [c], Hiroyuki Matsumoto [c], Yasushi Enokido [c], and Takashi Ogi [a †]

[a]Chemical Engineering Program, Department of Advanced Science and Engineering, Graduate School of Advanced Science and Engineering, Hiroshima University, 1-4-1 Kagamiyama, Higashi-Hiroshima, Hiroshima 739-8527, Japan

[b]Chemical Engineering Department, Universitas Internasional Semen Indonesia, Kompleks PT. Semen Indonesia (Persero) Tbk, Jl. Veteran, Gresik 61122 East Java, Indonesia

[c]Materials Research Center, Technology & Intellectual Property HQ, TDK corporation, 570-2 Matsugashita, Minami-Hadori, Narita, Chiba 286-8588, Japan

[†]Corresponding author: Takashi Ogi, ogit@hiroshima-u.ac.jp

Tel/Fax: +81-82-424-3765

Contents

1. Characteristics of FeNi particles in various precursor concentrations

In our previous report, the use of 25 vol% ethanol was useful to produce the spherical and submicron sized FeNi particles from its metal salt form. To increase the production rate, a preliminary experiment was conducted by applying various concentrations of the precursor solution, i.e., 0.2, 0.3, 0.4, and 0.6 mol/L. An increase of the solution concentration resulted in an increase of the metal oxide phase owing to an insufficient reduction agent. **Figure S1** shows spherical particles with the Fe and Ni atoms distributed uniformly from the precursor concentration of 0.2 mol/L, while Janus particles occurred in the two phases of FeNi and FeO from the precursor concentration of 0.6 mol/L. Consequently, the magnetic saturation flux density (B_s) value plummeted from 1.5 T to 0.9 T for the concentrations of 0.2 mol/L to 0.6 mol/L, as shown in **Figure S2** ·

2. Measurement of the hollow percentage by TEM image

Particle count from TEM images was used to determine the hollow percentage of the resulting particles as presented in **Figure S3**. We calculated the number of particles at least 400 particles. The amount of hollow and dense particles are summarized statistically in **Figure S4**.

3. Gas chromatography analysis

To confirm carbon formation as a side effect of the ethanol decomposition, gas chromatography analysis was conducted by using a Shimadzu GC-14B (Shimadzu, Japan) gas chromatograph equipped with a split/spitless injector. The chromatograms were recorded

and calculated by using a Shimadzu C-R8A (Shimadzu, Japan) computing integrator. The gas chromatography analysis shown in **Figure S5** depicts the gas composition in the flue gas from the fed solution droplet of 25 vol% ethanol into the spray pyrolysis reactor at 1200 °C.

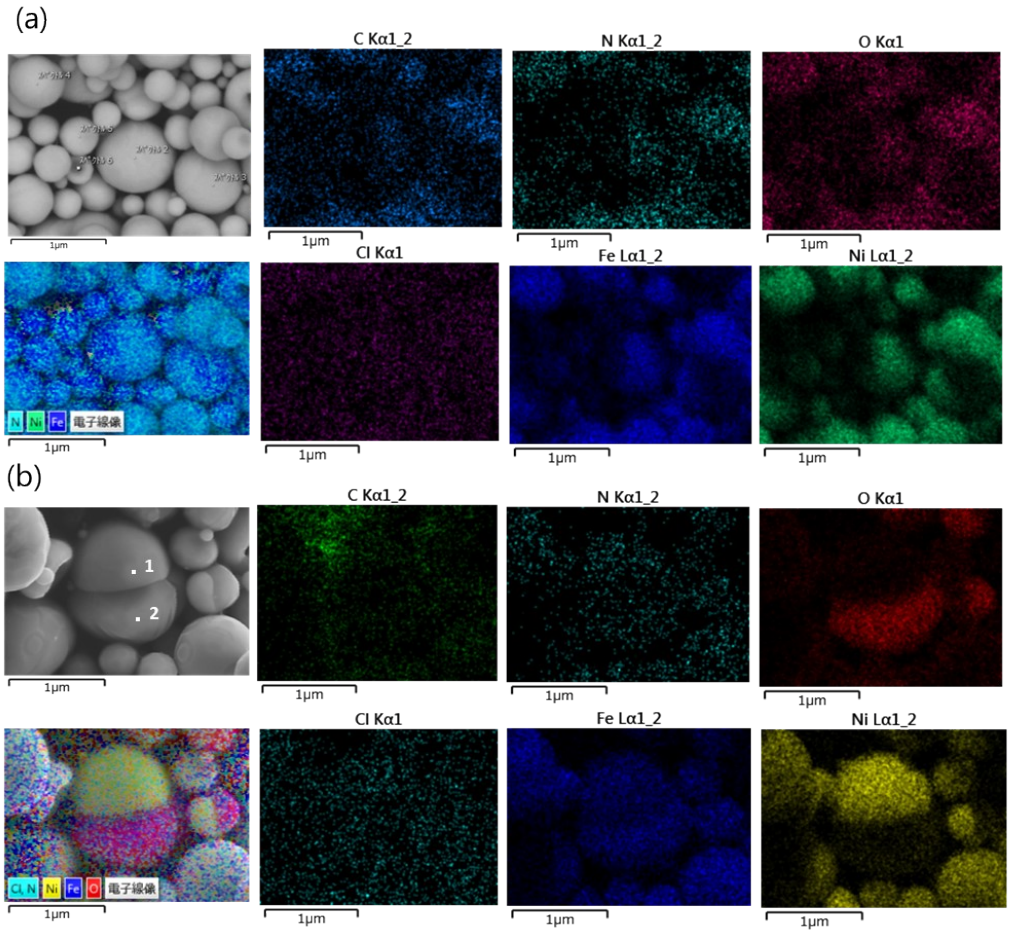

Figure S1. Elemental mapping of FeNi particles in different concentrations: (a) 0.2 mol/L; b) 0.6 mol/L.

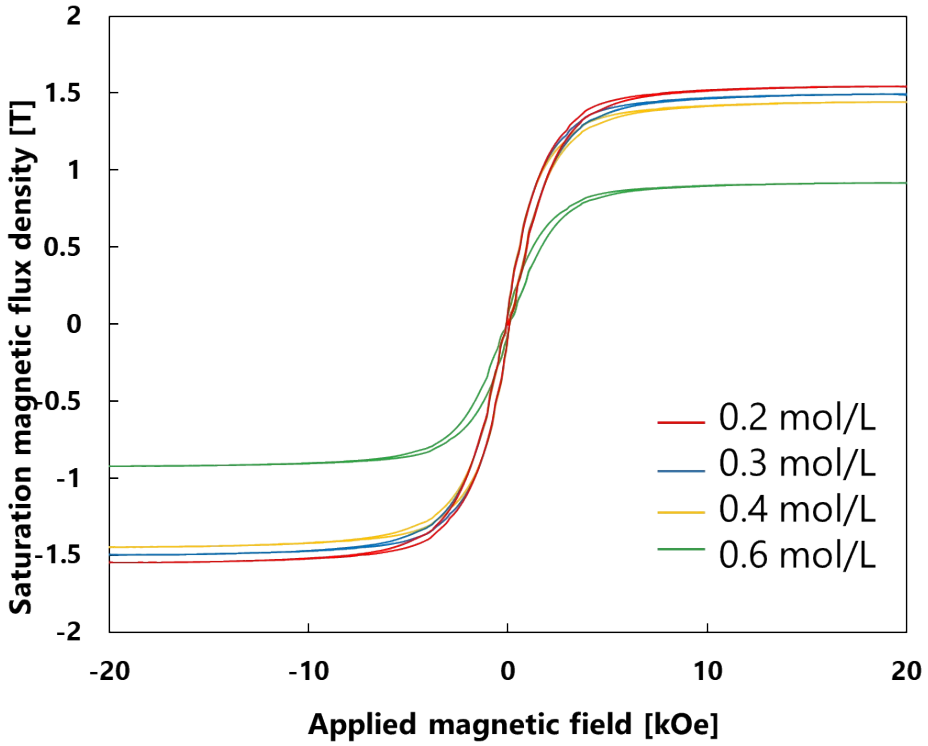

Figure S2. Magnetization characteristic of FeNi particles in various precursor concentrations.

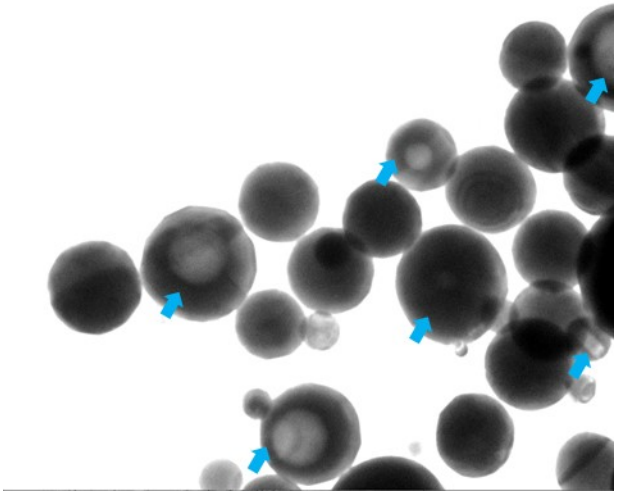

Figure S3. Calculating the hollow particle percentage from the TEM images. The blue arrow is indicating the hollow particles.

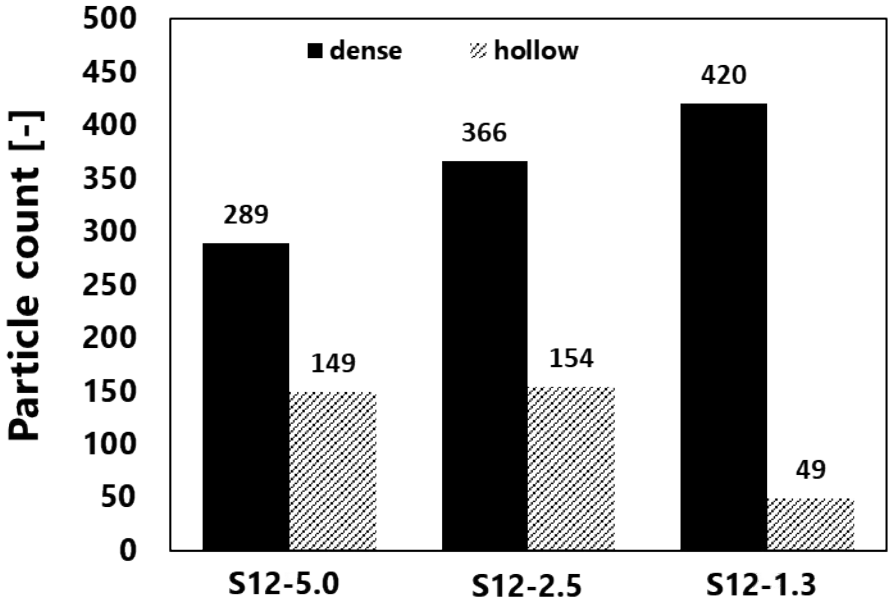

Figure S4. The bar chart of the dense and hollow FeNi particles count

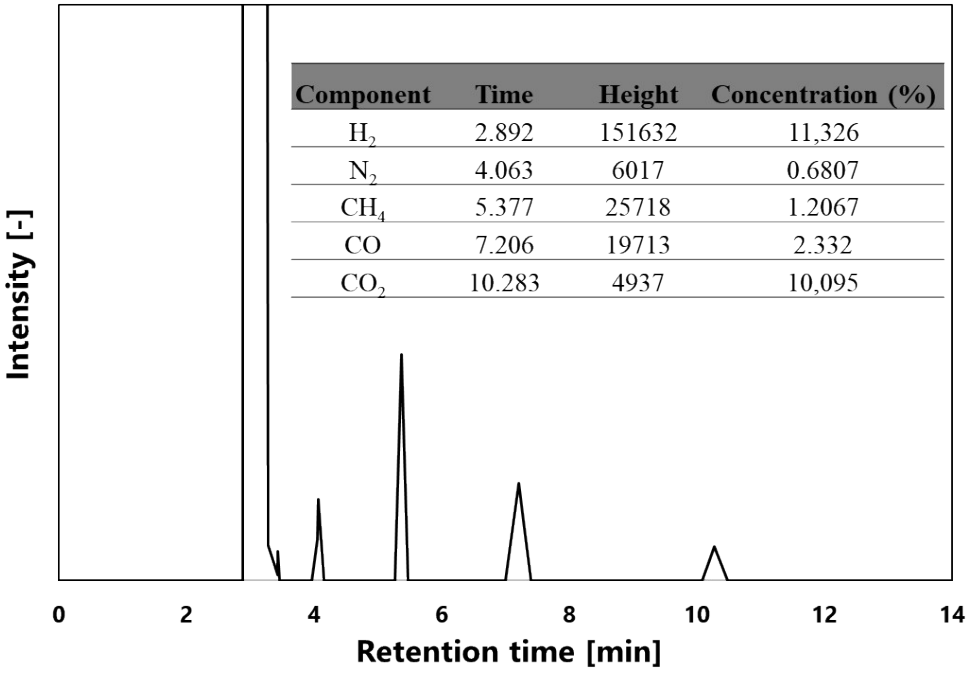

Figure S5. Gas chromatography analysis of the flue gas from 25 vol% ethanol–water.

4. Confirmation of the $L1_0$ phase of FeNi particles

An XRD pattern at a low angle was used to validate the presence of the hard magnetic material characteristic, which was most likely present in the FeNi based material. All of our samples were absent of the $L1_0$ phase of FeNi particles, as shown in **Figure S6**.

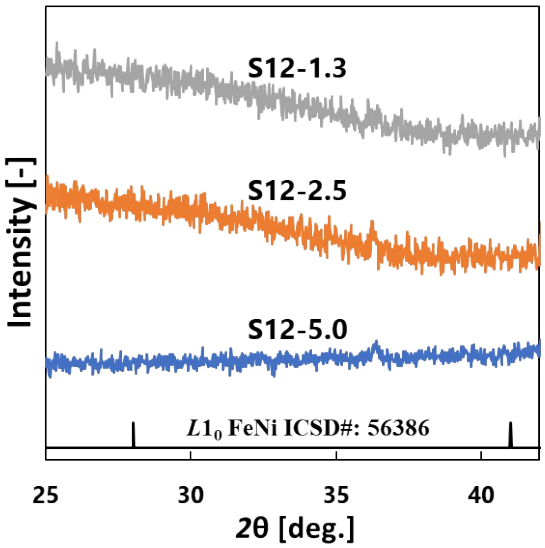

Figure S6. XRD pattern at a low angle of the submicron FeNi particles.

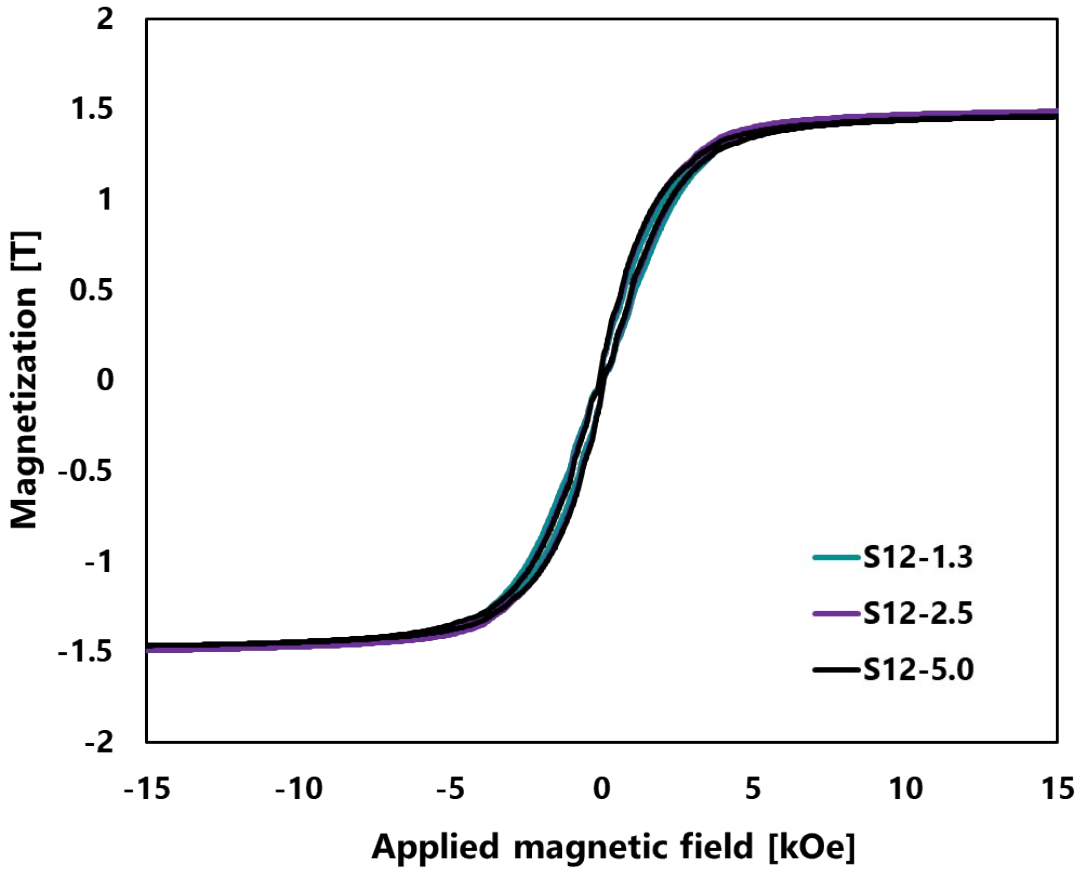

Figure S7. Hysteresis loop of FeNi particles in various carrier gas flow rates at 1200 °C.

5. Measurement of the adjacent non-magnetic region

The adjacent non-magnetic region was determined by measuring the distance between particles. The distance of each particle was measured in at least 4 directions, as shown in **Figure S8**, and then the average distance was calculated as the quantitative particle distance.

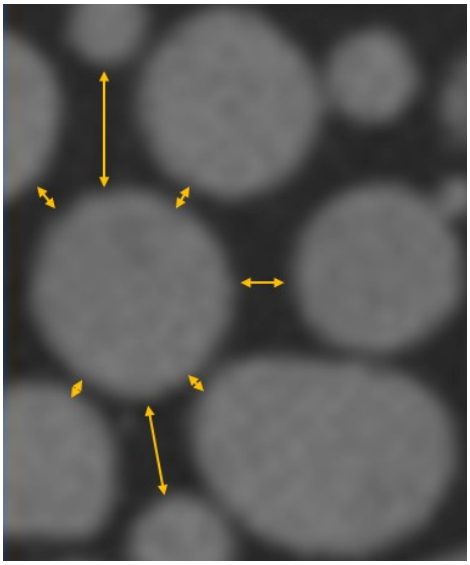

Figure S8. Schematic distance measurement for individual particles.